J Solid State Electrochem (2008) 12:679–686
DOI 10.1007/s10008-007-0401-6

ORIGINAL PAPER

# The processes involved in the Se electrodeposition and dissolution on Au electrode: the $H_2Se$ formation

**M. O. Solaliendres · A. Manzoli · G. R. Salazar-Banda · K. I. B. Eguiluz · S. T. Tanimoto · S. A. S. Machado**

Received: 10 April 2007 / Revised: 26 July 2007 / Accepted: 2 August 2007 / Published online: 6 September 2007


**Abstract** The processes involved in the Se electrodeposition, mainly the one related to the formation of $H_2Se$ species on Au electrode in perchloric acid solutions, have been investigated through cyclic voltammetry, electrochemical quartz crystal microbalance (EQCM), rotating ring-disc electrode (RRDE), and atomic force microscopy (AFM) techniques. In the experiments performed with the EQCM, with the potential sweep in the negative direction, the responses for the mass variation were divided in three well-defined potential regions: A (from 1.55 to 0.35 V), B (from 0.35 to −0.37 V), and C (from −0.37 to −0.49 V). It was verified that the following processes can occur, respectively: the species $(AuO)_2H_2SeO_3$ was desorbed during the AuO reduction, the reduction of Se(IV) to Se(0), and the formation of $H_2Se$. When the potential was swept in the positive direction, the responses for the mass variation were divided in four well-defined potential regions: D (from −0.49 to 0.66 V), E (from 0.66 to 0.99 V), F (from 0.99 to 1.26 V), and G (from 1.26 to 1.55 V), and the described processes in these regions were, respectively: the Se deposition and adsorption of water molecules and/or perchlorate ions, the Se dissolution, the Se incorporating mass in the form of HO–Se, and the Au oxidation (all potentials are referred to the Ag/AgCl electrode). Making use of the RRDE, using the collection technique, the formation of $H_2Se$ species during the Se electrodeposition was investigated. Therefore, it was confirmed that this species is formed on the disc electrode between −0.3 and −0.55 V vs the Ag/AgCl potential range (collecting the oxidized compound onto the ring electrode). AFM images also indicated that the surface topography of the Se-massive deposit on Au is different from the images registered after the formation of $H_2Se$ species, confirming the cathodic stripping of Se.

**Keywords** Selenium · Electrochemical · quartz crystal · microbalance · Gold · Electrodeposition · Rotating ring-disc electrode · Atomic force microscopy

M. O. Solaliendres
Departamento de Química,
Universidade Estadual de Mato Grosso do Sul,
CP 351, 79804-970,
Dourados, MS, Brazil

M. O. Solaliendres · A. Manzoli · G. R. Salazar-Banda (✉) · K. I. B. Eguiluz · S. T. Tanimoto · S. A. S. Machado
Instituto de Química de São Carlos, Universidade de São Paulo,
CP 780, 13560-970,
São Carlos, SP, Brazil
e-mail: gianrsb@gmail.com

## Introduction

Selenium is a semimetal found in different allotropic forms, the most common one is a red solid, consisting of $Se_8$ [1] molecules. Because of its good electrical conductiveness in the presence of light, Se has a high commercial value, especially in optoelectronics and chemical industries [2–4]. The main industrial applications of Se are related to its semiconducting properties, as it is appropriate to the conversion from solar into electric energy, with band gap between 1.5 and 3.0 eV [5–8].

Currently, there has been an increase in the interest for the Se electrodeposition, especially as a low-cost method for the metallic selenides preparation. This method allows the deposition of thin and ordered layers, which increase its efficiency in the conversion of luminous energy. The argument for applying of thin and ordered layers as precursors for the formation of semiconductor deposits is to avoid the tendency to obtain amorphous or polycrystal-

line "cauliflowers" deposits so called because of their convoluted morphology [9]. The extensive grain boundary networks in such materials increase their resistivity and provide recombination centers and are thus detrimental to most applications [10]. Moreover, the electrodeposition makes possible the formation of ordered layers mixing Se with other metals such as Zn and Pb, often used in photovoltaic devices [8–12].

One of the first works published about Se electrodeposition on Au substrate was carried out by Andrews and Johnson [13]. These authors used cyclic voltammetry (CV) experiments in $HClO_4$ 0.1 mol $L^{-1}$ and verified the existence of three distinct states of Se represented by three anodic peaks, which are relative to the dissolution of high amounts of the Se deposited. The formation of a bulk deposit of Se produces a large activity gradient, which is the driving force for irreversible diffusional transport of Se into the Au electrode, forming an Au–Se alloy of unknown stoichiometry.

Wei et al. [14] investigated the reduction of Se(IV) in $Na_2SO_4$ 0.5 mol $L^{-1}$ on Au substrates through CV and electrochemical quartz crystal microbalance (EQCM) techniques. The authors concluded that the direct six-electron reduction pathway (Se(IV)→Se(II−)) competes with the initial four-electron process. Coupling with a subsequent (fast) chemical reaction between Se(II−) and Se(IV) results in the further deposition of Se(O) at the electrode surface. The electrochemical behavior at more negative potentials reflected a complex interplay of the four-electron and six-electron reduction processes and the chemical reaction along with the effect of Se(II−) ions stripped from the initial selenium layer. Thus, the delicate balance between these is influenced by two variables: the potential and the Se(II−) concentration in the electrolyte.

In this sense, Alanyalioglu et al. [15] reported on the electrodeposition of Se atomic layers on Au(111) surfaces from aqueous $SeO_2$ solutions. The behavior of this system was complex and characterized by three voltammetric features preceding the onset of bulk Se deposition (cannot be considered true underpotencial deposition): two features associated with the conversion from adsorbed selenate species to adsorbed selenite (not to the formation of atomic layers of elemental Se) and a peak associated with the four-electron reduction (four-proton reduction of adsorbed selenite to Se).

Furthermore, Santos and Machado [16] studied the underpotential deposition (UPD) of Se on a Pt electrode in perchloric acid, using the EQCM technique. The anodic responses of mass variations were divided in three well-defined potentials regions (vs the hydrogen electrode in the same solution); the first one between 0.05 and 0.7 V was attributed to the water adsorption on Se previously deposited, the second region between 0.7 and 1.1 V was attributed to the dissolution of $Se+H_2O$, and the third region between 1.1 and 1.55 V was attributed to the Se dissolution and the Pt oxide formation.

At this point, in spite of the studies about Se electrodeposition discussed previously, some aspects about the interfacial processes knowledge still need to be investigated [16], such as the $H_2Se$ formation. Besides, morphologic aspects are usually omitted in reports about the Se electrodeposition, although these aspects are important when the goal is the use of Se layers as precursors for semiconductor devices.

Considering this, the aim of this work is to investigate in detail the Se electrodeposition and dissolution, especially the formation of the $H_2Se$ species on Au electrode in $HClO_4$ media, using CV, EQCM, and the rotating ring-disc electrode (RRDE). Furthermore, the morphology of the deposits was investigated through atomic force microscopy (AFM) measurements.

## Experimental

The solutions were prepared dissolving $SeO_2$ in $HClO_4$. All the reagents used presented analytical grade from Merck®, and the water used to prepare the solutions was purified by the Milli-Q system (Millipore, nominal resistivity: 18.2 MΩ $cm^{-1}$). The solutions were deaerated with high-purity $N_2$ (White Martins SS), and the experiments were carried out at room temperature, under atmospheric pressure.

A quartz crystal analyzer (Seiko EG&G model QCA-917), interfaced with the potentiostat model 273 EG&G Parc Instruments, and a microcomputer were used for the electrochemical measurements of the resonant frequency of the quartz crystal. An AT-cut quartz crystal of $f_o$=9 MHz covered on both sides with a Au film was used as the working electrode. The geometric area of the Au electrode was approximately 0.2 $cm^2$. This electrode was cleaned by immersion in $H_2SO_4$ solutions, followed by repetitive cathodic/anodic polarizations in $H_2SO_4$ 0.5 mol $L^{-1}$. The mass sensitivity of the quartz crystal was 800 Hz $\mu g^{-1}$, which was determined by using the copper potentiostatic electrodeposition ($H_2SO_4$ 1 mol $L^{-1}$+$CuSO_4$ 0.1 mol $L^{-1}$), in which the dissolution charge densities were used to calculate the mass values, and the resonant frequencies were measured experimentally. The difference observed between the experimental mass sensitivity and its theoretical value is attributed to the difference between the resonant frequency with the crystal oscillating in the vacuum and in the solution [17].

For the RRDE experiments, a Pt/Au ring-disc (Pine Instruments) with geometric areas of 0.0017 and 0.27 $cm^2$, respectively, was used. The efficiency of collection for the RRDE was $N$=0.211, determined using the $Fe^{2+}/Fe^{3+}$

reversible reaction, as described in the study of Machado et al. [18]. The rotating electrodes were polished with 0.3-μm alumina suspensions followed by careful rinsing with Milli-Q water. A Pine Model RDE4 bi-potentiostat, a Pine Model ASR rotator, and a Hewlett Packard model 7046B recorder were used in the rotating-electrode experiments. The reference electrode used in this work was a Ag/AgCl/KCl 3 mol $L^{-1}$ electrode, and the auxiliary one was a Pt foil with a geometric area of 1 $cm^2$. Moreover, the surface topography of the deposits was analyzed ex situ by an atomic force microscope Topometrix Explorer.

## Results and discussion

### Cyclic voltammetry and electrochemical quartz crystal microbalance experiments

Initially, experiments were carried out using both CV and EQCM to study the Se electrodeposition and electrodissolution processes. As a matter of fact, the simultaneous use of these techniques is a useful way for the elucidation and understanding of the chemical process involved in this kind of systems [14] (Se electrodeposition and dissolution).

Figure 1 shows the cyclic voltammogram (Fig. 1a) and the associated mass variation (Fig. 1b) responses recorded in a solution containing $SeO_2$ $2\times10^{-3}$ mol $L^{-1}$ and $HClO_4$ 0.5 mol $L^{-1}$ measured on the Au electrode of the quartz crystal. The experiment was carried out between +1.55 V (initial potential) and −0.49 V (inversion cathodic potential) at 0.05 V $s^{-1}$. Studying accurately Fig. 1a, the voltammetric peaks $I_c$ and $I_a$ can be associated with the processes of Au oxide reduction and Au oxidation, respectively [19]. The

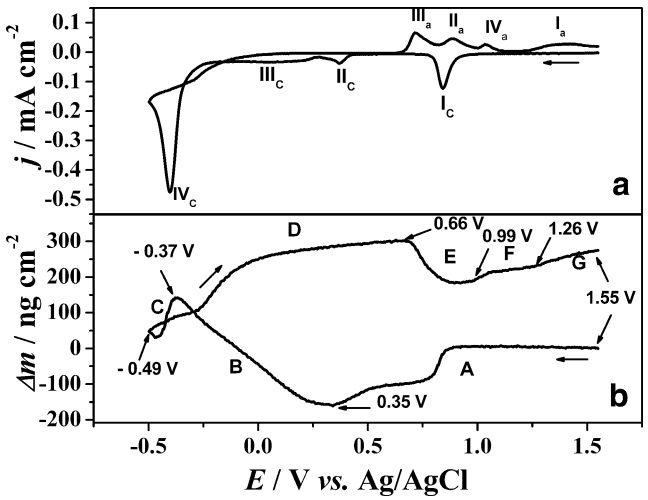


**Fig. 1** **a** *j–E* (cyclic voltammogram) and **b** Δ*m–E* (massogram) profiles for selenium electrodeposition and electrodissolution in the Au electrode of the quartz crystal, obtained at 0.05 V $s^{-1}$ in $HClO_4$ 0.1 mol $L^{-1}$+$SeO_2$ $2\times10^{-3}$ mol $L^{-1}$ solution

pair of peaks $II_c$ and $II_a$ is usually associated with the Se UPD [20, 21], and the processes $III_c$ and $III_a$ are related to the Se massive deposition and dissolution, respectively [20]. While, the peak $IV_c$ is due to the formation of $H_2Se$, commonly described as [16, 22]:

$$Se + 2H^+ + 2e^- \rightarrow H_2Se_{(g)} \quad (1)$$

Nevertheless, some authors suggested that at more negative potentials, the formation of the $H_2Se$ species for the direct reduction of Se (IV) to Se (II−) also occurs, with transference of six electrons, in accordance with the Eq. 2 [23]:

$$H_2SeO_3 + 6H^+ + 6e^- \rightarrow H_2Se + 3H_2O \quad (2)$$

Meanwhile, the process $IV_a$ has been associated with the formation of a Se–Au intermetallic complex of unknown stoichiometry [13].

Simultaneously, the Δ*m–E* profile in Fig. 1b shows three regions of mass variation during the negative scan from +1.55 to −0.49 V: A (from +1.55 to +0.35 V), B (from +0.35 to −0.37 V), and C (from −0.37 to −0.49 V).

The region A (from +0.9 V to +0.35 V) is characterized by a sharp mass diminishing in the beginning and a more smooth decrease after +0.82 V. Between 0.35 and −0.37 V, region B, an increase of the mass is observed, which is attributed to the Se-massive electrodeposition process. Between −0.37 and −0.49 V (region C), where the current peak $IV_c$ is observed, the mass decreased rapidly. When the potential value was more negative than −0.39 V, the cathodic current decreased to reach a limit value at −0.49 V, and the mass remained approximately constant until it reached the inversion cathodic potential. These facts could be associated with selenium electrodeposition and hydrogen evolution reaction (HER) on the Au electrode. It is possible to observe that the current remains cathodic up to the potential of about 0 V during the reverse scan.

During reverse scan, the voltammetric response reveals the presence of four anodic peaks ($I_a$, $II_a$, $III_a$, and $IV_a$), which could be associated with the Au oxidation, the Se adatoms dissolution on Au electrode (UPD), the massive Se dissolution, and to the formation of a Se–Au intermetallic compound with undetermined stoichiometry, respectively. Simultaneously, the Δ*m–E* profile in Fig. 1b shows four regions with mass variation during the reverse scan (from −0.49 to +1.55 V): D (from −0.49 to 0.66 V), E (from +0.66 to +0.99 V), F (from +0.99 V to +1.26 V), and G (from +1.26 to +1.55 V).

Within region D, between −0.49 and 0 V, both current and mass increase slightly. This situation indicates that the Se electrodeposition process on Se (electrodeposited on previous regions) is reinitiated because the HER rate on Se at this region was diminished. Between the potential range of 0 and 0.66 V, in the end of region D, the mass remained

almost constant (increasing slightly), and the current was maintained close to 0 mA $cm^{-2}$. When the potential was more positive than +0.66 V, region E, the anodic current peaks $II_a$ and $III_a$ appeared. These peaks corresponded to the stripping of Se to Se (IV), and consequently, in this region, a mass decrease is observed. In regions F and G, the mass increase observed could be associated with the oxidation of the adsorbed Se and Au, respectively.

For an accurate study of the process occurring on the Au electrode of the quartz crystal in the previous defined potential regions, a plot of mass variation vs charge density ($\Delta m$ vs $\Delta q$) is presented in Fig. 2. It is important to point out that the charge density was calculated by the integration of $j$ (current density) with the time. In this calculation, using the Faraday law, the mass and charge are associated by the number of electrons transferred in the processes and by the molecular weight of the reacting species (Eq. 3) [24].

$$\left(\frac{\Delta m}{\Delta q}\right)F = \frac{M}{z} \tag{3}$$

where $M$ is the molar mass of the adsorbed/desorbed species (or deposited), $z$ is the number of electrons involved in the process, and $F$ is the constant of Faraday (96,487 C $mol^{-1}$).

In region A (Fig. 2), between +0.9 and +0.35 V, a mass decrease is observed, which corresponds to −167 ng $cm^{-2}$, much larger than that one for AuO reduction (−32 ng $cm^{-2}$) [19, 25]. This means that more species must be dissolving, without involving charge transfer. The scheme presented as Scheme 1 was previously postulated [26] for this region A when the ZnSe electrodeposition from an acid bath containing Zn(II) and Se(IV) using voltammetric and nanogravimetric techniques was studied. Thus, these electrode processes may occur with the $SeO_2$ in acid solution, as the

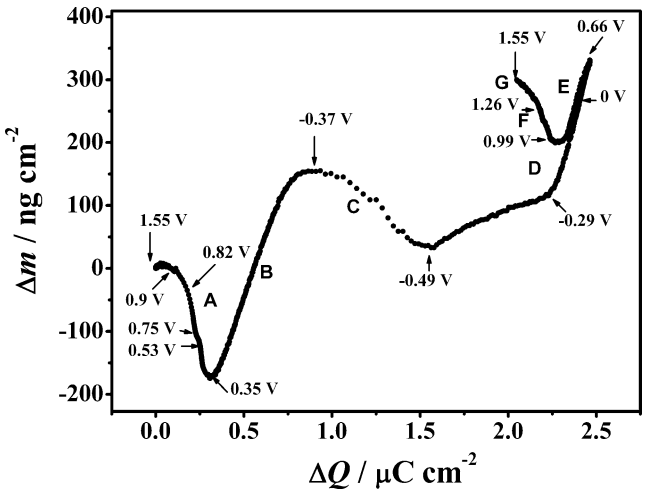


**Fig. 2** $\Delta m$ vs $\Delta q$ relationship with values obtained from the $j$–$E$ and the $\Delta m$–$E$ profiles shown in Fig. 1

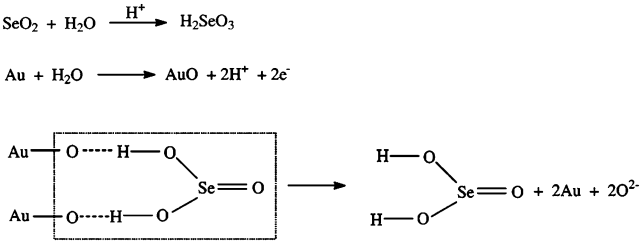


**Scheme 1** Reaction scheme for region A in Fig. 2

electrode surface is polarized at highly positive potentials, in the initial potential of Fig. 2. The desorption of these species (Scheme 1) demands theoretically −161 ng $cm^{-2}$, which is very close to the mass diminishing observed in Fig. 2.

Region B presents two pairs of peaks in the voltammetric response of Fig. 1a associated with the UPD and massive deposition of Se and only a slope in the mass response of Fig. 1b, which corresponds to a mass increase of about 320 ng $cm^{-2}$. As a deposition of one monolayer of Se corresponds to 78.9 ng $cm^{-2}$ (Se atomic mass × moles of active sites on the Au surface [$2\times10^{-9}$ mol $cm^{-2}$ [27]]), the mass variation in this region corresponds to four monolayers of Se. From Fig. 2, an $M/z$ value of 15 g $mol^{-1}$ was obtained ($1.6\times10^{-4}$ g $C^{-1}\times$96,487 C $mol^{-1}$). Therefore, as the Se deposition is represented by Eq. 4 [20], a lower value of $M/z$ is observed experimentally. This feature could be due to the fact that in the beginning of the Se deposition, within the UPD region, simultaneous desorption of perchorate and water can be occurring, which were not completely dissolved in the preceding region, which diminished, in this way, the slope value for the Se electrodeposition.

$$\begin{aligned} &H_2SeO_{3\,(aq)} + 4H^+ + 4e^- \rightarrow Se^0 + 3H_2O \\ &M/z = 19.74\,\mathrm{g\,mol^{-1}} \end{aligned} \tag{4}$$

For region C, which corresponds to the $H_2Se$ formation region, an effective $M/z$ value of 4.5 g $mol^{-1}$ ($4.65\times10^{-5}$ g $C^{-1}\times$96,487 C $mol^{-1}$) was obtained from Fig. 2. This value was lower than the theoretical one (39.48 g $mol^{-1}$) for the reduction of Se(0) to $H_2Se$ in an electronic process involving two electrons, described in Eq. 1.

A reason for the $M/z$ reduction in region C is that at more negative potentials, the formation of $H_2Se$ species for the direct reduction of Se(IV) also occurs, with transference of six electrons, in accordance with the Eq. 2, in which the effective $M/z$ value is zero, as there is no deposition.

Kemell et al. [28] obtained an effective $M/z$ value of 5.50 g $mol^{-1}$ for the formation of the $H_2Se$ species, in a solution of Se deposition that contained $HSeO_3^-$. The effective $M/z$ value is also lower than the theoretical value (39.48 g $mol^{-1}$). The same authors, when studied the formation of $H_2Se$ on a Se film previously deposited in

the absence of $H_2SeO_3$, obtained the effective *M*/*z* value of 37.57 g $mol^{-1}$, which is next to the theoretical value that evidenced the formation of the $H_2Se$ species through Eq. 1.

In Fig. 1a, the charge associated with the peak of massive Se dissolution ($III_a$) decreases when the deposition potential is more negative. This fact is an indication that $H_2Se$ formation occurs preferentially by means of the Eq. 1. Moreover, when the value of the potential is more negative than −0.37 V (between −0.37 and −0.45 V), the cathodic current decreases, indicating exhaustion of the Se deposited, conversely to the expected behavior considering the direct reduction as shown in Eq. 2.

Another reason for the reduction in the effective *M*/*z* value in region C is that at more negative potentials (between −0.45 and −0.49 V), the simultaneous Se deposition in accordance with the Eq. 5 also occurs.

$$H_2SeO_3 + H_2Se \rightarrow 3Se + 3H_2O \quad (5)$$

Furthermore, a mass loss of −118 ng $cm^{-2}$ is observed in region C, as discussed previously. Nevertheless, a complete monolayer of Se corresponds to 78.9 ng $cm^{-2}$, and therefore, the desorption of 1.5 monolayers of Se was observed, evidencing that the Se previously deposited was dissolved to form $H_2Se$ according to Eq. 1.

In region D (from −0.49 to 0.66 V) of Fig. 2, specifically in the beginning (from −0.49 to −0.29 V), a low effective *M*/*z* value was observed (2.5 g $mol^{-1}$), calculated by $2.6\times10^{-5}$ g $C^{-1}\times96{,}487$ C $mol^{-1}$, suggesting that the speed of the Se deposition according to Eq. 4 and the formation of $H_2Se$ according to Eq. 1 are approximately the same. In this region, a mass increase of 82 ng $cm^{-2}$ was observed, which corresponds to one monolayer of Se deposited. Between −0.29 and 0 V, it was observed that the *M*/*z* value increased to 19 g $mol^{-1}$ ($2.04\times10^{-4}$ g $C^{-1}\times96{,}487$ C $mol^{-1}$), and this is an indication that in this region, the Se deposition predominates in accordance with Eq. 4, as the potential is not negative enough for the reduction of Se(0) to Se(II−) for Eq. 1. A mass increase of 148 ng $cm^{-2}$ was obtained corresponding to 1.9 monolayer of Se. Furthermore, between 0 V and 0.66 V, the effective M/z value increased to 22 g $mol^{-1}$ ($2.32\times10^{-4}$ g $C^{-1}\times96487$ C $mol^{-1}$), suggesting that a simultaneous adsorption of water and/or electrolyte anions is taking place.

In the region of the Se dissolution (region E), between 0.66 and 0.99 V, the effective *M*/*z* value was 20 g $mol^{-1}$ ($2.1\times10^{-4}$ g $C^{-1}\times96487$ C $mol^{-1}$), proving that in this region, the Se dissolution occurs. As a consequence, a mass decrease of −124 ng $cm^{-2}$, corresponding to 1.6 monolayers, of Se desorption is observed.

It is important to mention that 6.9 monolayers of Se were deposited in regions B (from 0.35 to −0.37 V) and D (from −0.49 to 0 V). Meanwhile, only 3.1 monolayers of Se were dissolved in the regions C (from −0.37 to −0.49 V) and E (from +0.66 to +0.99 V), thereby, Se remained adsorbed on the Au surface after region E.

Region F (from +0.99 to +1.26 V) was associated with Se-adsorbed oxidation, and effective *M*/*z* value of 16 g $mol^{-1}$ ($1.66\times10^{-4}$ g $C^{-1}\times96{,}487$ C $mol^{-1}$) corresponds to the theoretical value ($HO^-$=17 g $mol^{-1}$) for the HO–Se–OH formation [16]. These calculations confirm that complete Se dissolution does not occur in region E. For this reason, the Se ad-atoms, which remained on the surface, incorporated mass according to Eq. 6. Then, the formation of a Se–Au alloy was not observed.

$$HO - Se_{(ads)} + H_2O \rightarrow HO - Se_{(ads)} - OH + 1H^+ + 1e^- \quad M/z = 17\,g\,mol^{-1} \quad (6)$$

For region G (from +1.26 to +1.55 V) associated with the Au oxidation, the effective *M*/*z* value was 7 g $mol^{-1}$ (7.2×

**Table 1** Reactions sequence for the interfacial processes identified using the EQCM and their potential range

| Region | Potential range | Equation |
|---|---|---|
| A | + 0.9 and + 0.35 V | Scheme 1 |
| B | +0.35 V and −0.37 V | $H_2SeO_{3\,(aq)} + 4H^+ + 4e^- \rightarrow Se^0 + 3H_2O$ |
| C | −0.37 and −0.45 V | $Se^0 + 2H^+ + 2e^- \rightarrow H_2Se_{(g)}$ |
| | | $H_2SeO_3 + 6H^+ + 6e^- \rightarrow H_2Se + 3H_2O$ |
| | | $Se^0 + 2H^+ + 2e^- \rightarrow H_2Se_{(g)}$ |
| | −0.45 and −0.49 V | $H_2SeO_3 + 6H^+ + 6e^- \rightarrow H_2Se + 3H_2O$ |
| | | $H_2SeO_3 + H_2Se \rightarrow 3Se + 3H_2O$ |
| D | −0.49 and −0.29 V | $H_2SeO_{3\,(aq)} + 4H^+ + 4e^- \rightarrow Se^0 + 3H_2O$ |
| | | $Se^0 + 2H^+ + 2e^- \rightarrow H_2Se_{(g)}$ |
| | −0.29 and 0 V | $H_2SeO_{3\,(aq)} + 4H^+ + 4e^- \rightarrow Se^0 + 3H_2O$ |
| | 0 V and +0.66 V | $H_2SeO_{3\,(aq)} + 4H^+ + 4e^- \rightarrow Se^0 + 3H_2O$ |
| | | simultaneous adsorption of water and/or electrolyte anions |
| E | +0.66 and +0.99 V | $Se^0 + 3H_2O \rightarrow H_2SeO_{3(aq)} + 4H^+ + 4e^-$ |
| F | +0.99 to +1.26 V | $HO - Se_{(ads)} + H_2O \rightarrow HO - Se_{(ads)} - OH + 1H^+ + 1e^-$ |
| G | +1.26 to +1.55 V | $2Au^0 + 6OH^- + 4e^- \rightarrow Au_2O_{3\,(s)} + 3H_2O$ |

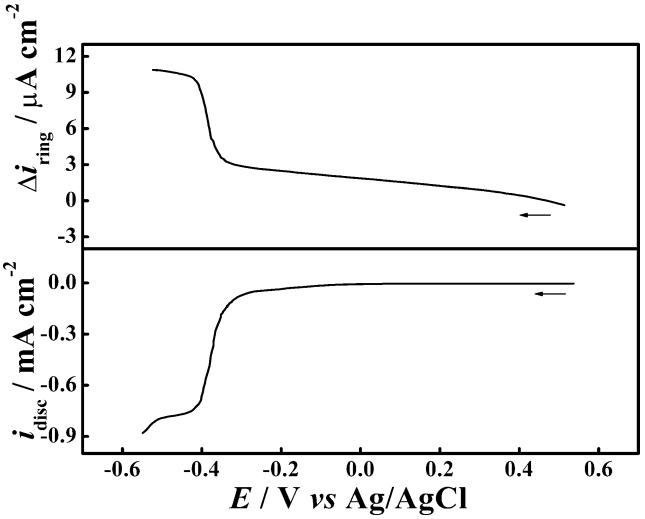


**Fig. 3** Linear sweep voltammetric response for the Au disc electrode (first cycle) in $HClO_4$ 0.1 mol $L^{-1}$+$SeO_2$ $2\times10^{-3}$ mol $L^{-1}$ solution at 0.05 V $s^{-1}$; $\omega$=1,600 rpm and the corresponding Pt ring current variation. The ring was kept polarized at 1.0 V

$10^{-5}$ g $C^{-1}\times96{,}487$ C $mol^{-1}$), referring to the O incorporation on the Au surface, according Eq. 7.

$$2Au^0 + 6OH^- + 4e^- \rightarrow Au_2O_{3\,(s)} + 3H_2O \qquad M/z = 8.0\,\mathrm{g\,mol^{-1}} \tag{7}$$

Finally, the reactions sequence for the interfacial processes identified using the EQCM and their potential range is presented in Table 1.

## Rotating ring-disc electrode studies

The investigation of the $H_2Se$ formation (reduction from $Se_{ads}$ to Se(II−)) during the Se electrodeposition was also performed using a RRDE Pt/Au with the collection method (Fig. 3). In this study, the experiments were performed at 1,600 rpm in a solution of $HClO_4$ 0.1 mol $L^{-1}$ containing $SeO_2$ $2\times10^{-3}$ mol $L^{-1}$. The Au-disc electrode was scanned between 0.54 and −0.55 V at 0.05 V $s^{-1}$, while the Pt-ring electrode was polarized at 1.0 V. Concerning to this, the ring is polarized in an adequate potential so that the Se(II−) produced on the disc (from $H_2Se$) can be collected in the ring under the form of Se(0) (oxidation from $H_2S$ to Se(II−)). The current variation observed in the ring follows the disc profile, once it is originated through oxidation of the species formed ($H_2Se$) on the disc electrode, which can form not only Se(0) but also Se(IV).

As the disc potential was scanned toward the cathodic direction, no Se(IV) should be produced. Then, the only possible process on the disc should be the reduction of Se (0) to Se(II−), generating $H_2Se$, which is a gas at room temperature. Therefore, this species when released from the disc is collected in the ring and oxidized to Se(0), according to Eq. 8a, or to Se(IV), according to Eq. 8b.

$$H_2Se \rightarrow Se(0) + 2H^+ + 2e^- \tag{8a}$$

$$H_2Se \rightarrow H_2SeO_3 + 6H^+ + 6e^- \tag{8b}$$

Through the calculation of the disc and ring charge densities, in the formation interval of the $H_2Se$ species (from −0.30 to −0.55 V), it is possible to investigate which process is happening in the system (Eqs. 8a or 8b). For reaction 8a, the charge density correspondents to two electrons, and for reaction 8b, it corresponds to six electrons. If the charge density calculated for the disc is the same as the charge density calculated for the ring, the reaction that occurs is Eq. 8a. However, if the charge density calculated for the disc is lower than the one calculated for the ring (one of three), the reaction that occurs is Eq. 8b.

The value obtained for the charge density collected in the ring was 10 mC $cm^{-2}$, and the corresponding value for the deposition on the disc was also 10 mC $cm^{-2}$. This indicates that the species collected in the ring (i.e., $H_2Se$) is oxidized to Se(0), according to the reaction 8a. The disc

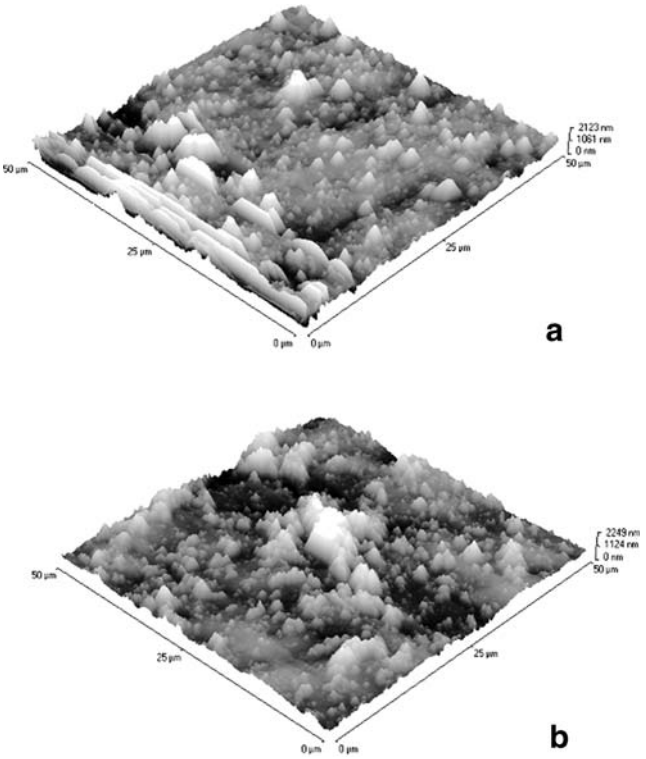


**Fig. 4** AFM images (50×50 μm) of Au substrates covered with deposited of: **a** massive Se deposited maintaining the electrode potential at 0 V during 1,500 s and **b** massive Se, in the region of $H_2Se$ formation, deposited at −0.40 V by 15 s. Solution for the deposition: $HClO_4$ 0.1 mol $L^{-1}$+$SeO_2$ $2\times10^{-3}$ mol $L^{-1}$, area of electrodes=0.27 $cm^2$

and the ring charge density values are increased, indicating a massive dissolution process of Se in the $H_2Se$ formation.

### Atomic force microscopy

The AFM technique was also used to confirm the formation of $H_2Se$ in potentials more negative than −0.3 V. Therefore, AFM was used to show differences in the topography of the Se-massive deposit and the Se deposit with the $H_2Se$ formation. Then, the Se film was deposited electrochemically on two situations: at 0 V by 1,500 s and at −0.4 V by 15 s. AFM images of Se massive deposition and with the formation of $H_2Se$ are shown in Figs. 4a and b, respectively, for a scan area of 50×50 μm.

In the Fig. 4a recorded at 0 V (outside the range of $H_2Se$ formation) by 1,500 s, the topology of the film observed is regular with the presence of some clusters with sizes between 1 and 5 μm and some agglomerates with size higher than 5 μm. On the other hand, the mixed deposition of Se with the $H_2Se$ formation (Fig. 4b) causes a change in the film morphology. The clusters were deposited more irregularly and the film showed some cavities or sites without deposit, probably because of the Se (previously deposited) reaction to form $H_2Se$. Furthermore, in the experimental conditions employed in this work, the $H_2Se$ (gas) diffuses toward the solution phase, generating hollows on the deposit surface of the Se deposit, confirming the cathodic stripping of Se.

## Conclusions

In this paper, the Se electrodeposition on the Au electrode in the $HClO_4$ solution was studied through CV, EQCM, RRDE, and AFM techniques. Through the experiments with the EQCM, it was possible to detect the Se deposition and the adsorption and desorption of nonelectroative molecules, such as water and/or $ClO_4^-$, during the process of Se electrodeposition. It was also possible to observe that the formation of the $H_2Se$ species occurs mainly according to the process described in the Eq. 1 ($Se + 2H^+ + 2e^- \rightarrow H_2Se_{(g)}$), with transference of two electrons, but the formation of this species can also occur with the transference of six electrons, at more negative potentials, according to the Eq. 2 ($H_2SeO_3 + 6H^+ + 6e^- \rightarrow H_2Se + 3H_2O) M/z = 0$, and still in more negative potentials (between −0.45 and −0.49 V), the Se deposition occurs by means of the chemical reaction of Eq. 5: $H_2SeO_3 + H_2Se \rightarrow 3Se + 3H_2O$. Moreover, the Se complete dissolution was not observed, and the ad-atoms still remained on the Au, forming the respective oxide in the potential region from +0.99 to +1.26 V, according to Eq. 6 ($HO - Se_{(ads)} + H_2O \rightarrow HO - Se_{(ads)} - OH + 1H^+ + 1e^-$). Then, within this potential region, the formation of an intermetallic complex Se–Au of unknown stoichiometry was not observed. The use of the RRDE permitted to prove the $H_2Se$ formation during the Se electrodeposition at high cathodic potentials (from −0.30 to −0.55 V vs Ag/AgCl). The Se(II−) was collected in the ring as Se(0), according to the reaction of the Eq. 8a ($H_2Se \rightarrow Se(0) + 2H^+ + 2e^-$). The AFM technique also confirmed the formation of $H_2Se$ in potentials more negative than −0.3 V vs Ag/AgCl. Thus, the mixed deposition of Se with the $H_2Se$ formation causes a change in the film morphology (cavities and sites without Se deposit) when compared with the regular deposit obtained outside the range of $H_2Se$ formation potentials (from −0.30 to −0.55 V). Therefore, the AFM images showed that $H_2Se$ species change the Se electrodeposition process on the Au surface. The experimental results obtained in this work allowed a more complete interpretation about the electrode processes involved in the Se electrodepositon and electrodissolution, illustrating how important it is to use the CV and EQCM techniques. This study will be useful for the development of electrochemical methodologies, which can be used for the development of semiconducting compounds, such as ZnSe, which will be studied in further experimental works.

**Acknowledgements** The authors would like to thank to the National Counsel of Technological and Scientific Development-CNPq and The State of São Paulo Research Foundation-FAPESP (Processes: 03/03221-6 and 06/50692-2) for the financial support.

## References

1. Gissler W (1980) J Electrochem Soc 127:1713
2. Zhdanov SI (1975) In: Bard AJ (ed) Encyclopedia of electrochemistry of the elements, vol 4. Dekker, New York
3. Yesugade NS, Lokhande CD, Bhosale CH (1995) Thin Solid Films 263:145
4. Kazacos MS, Millar B (1980) J Electrochem Soc 127:2378
5. Massaccesi S, Sanchez S, Vedel J (1996) J Electroanal Chem 412:95
6. Pandey RK, Sahu SN, Chandra S (1996) Handbook of semiconductor electrodeposition. Marcel Dekker, New York
7. Benamar E, Rami M, Fahoume M, Chraibi F, Ennaqui A (1999) Solid State Sci 1:301
8. Savadogo O (1998) Sol Energ Mat Sol C 52:361
9. Tomkiewicz M, Ling I, Parsons WS (1982) J Electrochem Soc 129:2016
10. Chartier P, Ba B, Ebothe J, Vante NA, Cong HN (1982) J Electroanal Chem 138:381
11. Riveros G, Henríquez R, Córdova R, Schrebler R, Dalchiele EA, Gómez H (2001) J Electroanal Chem 504:160
12. Pejova B, Grozdanov I (2001) Appl Surf Sci 177:152
13. Andrews RW, Johnson DC (1975) Anal Chem 47:294
14. Wei C, Myung N, Rajeshwar K (1994) J Electroanal Chem 375:109

15. Alanyalioglu M, Demir U, Shannon C (2004) J Electroanal Chem 561:21
16. Santos MC, Machado SAS (2004) J Electroanal Chem 567:203
17. Gabrielli C, Keddam M, Torresi RM (1991) J Electrochem Soc 138:2657
18. Machado SAS, Tanaka AA, Gonzalez ER (1991) Electrochim Acta 36:1325
19. Shibata M, Kobayashi T, Furuya N (1997) J Electroanal Chem 436:103
20. Fonticelli MH, Posadas D, Tucceri RI (2004) J Electroanal Chem 565:359
21. Modolo R, Traore M, Vittori O (1986) Electrochim Acta 31:859
22. Furuya N, Matoo S (1979) J Electroanal Chem 98:189
23. Zuman P, Somer G (2000) Talanta 51:645
24. Sauerbrey G (1959) Zeitschrift für Physic 155:206
25. Wei C, Myung N, Rajeshwar K (1993) J Electroanal Chem 347:223
26. Manzoli A, Santos MC, Machado SAS (2007) Thin Solid Films 515:6860
27. Mori E, Baker CK, Reynolds JR, Rajeshwar K (1988) J Electroanal Chem 252:441
28. Kemell M, Saloniemi H, Ritala M, Leskelä M (2000) Electrochim Acta 45:3737